Nanoscale

PAPER

View Article Online
View Journal | View Issue

Cite this: *Nanoscale*, 2024, **16**, 10819

Non-uniform magnetic fields for single-electron control

Mauro Ballicchia, * Clemens Etl, Mihail Nedjalkov and Josef Weinbub

Controlling single-electron states becomes increasingly important due to the wide-ranging advances in electron quantum optics. Single-electron control enables coherent manipulation of individual electrons and the ability to exploit the wave nature of electrons, which offers various opportunities for quantum information processing, sensing, and metrology. Here we explore non-uniform magnetic fields, which offer unique mechanisms for single-electron control. Considering the modeling perspective, conventional electron quantum transport theories are commonly based on gauge-dependent electromagnetic potentials. A direct formulation in terms of intuitive electromagnetic fields is thus not possible. In an effort to rectify this, a gauge-invariant formulation of the Wigner equation for general electromagnetic fields has been proposed [M. Nedjalkov *et al.*, *Phys. Rev. B*, 2019, **99**, 014423]. However, the complexity of this equation requires the derivation of a more convenient formulation for linear electromagnetic fields [M. Nedjalkov *et al.*, *Phys. Rev. A*, 2022, **106**, 052213]. This formulation directly includes the classical formulation of the Lorentz force and higher-order terms, depending on the magnetic field gradient, that are negligible for small variations of the magnetic field. In this work, we generalize this equation in order to include a general, non-uniform electric field and a linear, non-uniform magnetic field. The thus obtained formulation has been applied to investigate the capabilities of a linear, non-uniform magnetic field to control single-electron states in terms of trajectory, interference patterns, and dispersion. This has led to the exploration of a new type of transport inside electronic waveguides based on snake trajectories and the possibility of splitting wavepackets to realize edge states.

Received 14th November 2023,
Accepted 6th May 2024

DOI: 10.1039/d3nr05796h

rsc.li/nanoscale

1 Introduction

The field of electron quantum optics studies and applies electromagnetic (EM) field-controlled phenomena for manipulating electron states in solid-state quantum systems.[1–5] Ideally, transport theories should describe both processes governing electron trajectories and wave phenomena such as interference and diffraction in multiple dimensions. Theories based on EM potentials rely on formal mathematical apparatus related to the choice of scalar and vector potentials, which, however, obscures the physical aspects and thus the heuristic understanding of electron evolution. This is also true for the Wigner theory which among the alternative formulations of quantum mechanics utilizes classical concepts of a phase space and a quasi-distribution function. Indeed, the underlying Wigner quantum mechanics is formulated in electrostatic terms under the choice of zero vector potential.[6] The central quantities in the derived evolution (transport) equation are the Wigner function f_w and the Wigner potential V_w, defined by the Weyl transform of the density matrix and the scalar potential, respectively. The inclusion of the magnetic field, however, introduces additional terms, which depend on the choice of the gauge.[7–17] Six decades ago, Stratonovich[18] generalized the Weyl transform to replace the canonical momentum as a phase space coordinate with the kinetic momentum. The latter, being a physical quantity, is gauge invariant, and so is the transport equation for f_w derived by the Weyl–Stratonovich transform. Details can be found, *e.g.*, in ref. 19–21 and the references therein. The potentials are completely removed from the theory, which offers the advantage of depending only on physical factors, such as the EM fields **E** and **B**. The equation is mathematically challenging as it depends on multi-dimensional integrals of f_w with the terms

$$D^{\mathrm{F}}(\mathbf{E};\mathbf{r},\mathbf{p},\tau) = -\int \mathrm{d}\mathbf{s} e^{-\frac{i}{\hbar}\mathbf{p}\mathbf{s}}\left(\mathbf{s}\cdot\mathbf{E}\left(\mathbf{r}+\frac{\mathbf{s}\tau}{2}\right)\right)$$

$$H^{\mathrm{F}}(\mathbf{B};\mathbf{r},\mathbf{p},\tau) = \int \mathrm{d}\mathbf{s} e^{-\frac{i}{\hbar}\mathbf{p}\mathbf{s}}\left[\mathbf{s}\times\mathbf{B}\left(\mathbf{r}+\frac{\mathbf{s}\tau}{2}\right)\right]$$

$$I^{\mathrm{F}}(\mathbf{B};\mathbf{r},\mathbf{p},\eta,\tau) = \int \mathrm{d}\mathbf{s} e^{-\frac{i}{\hbar}\mathbf{p}\mathbf{s}}\left(\mathbf{s}\times\mathbf{B}\left(\mathbf{r}+\frac{\mathbf{s}\eta}{2}\right)\right) \cdot \left(\mathbf{s}\times\mathbf{B}\left(\mathbf{r}+\frac{\mathbf{s}\tau}{2}\right)\right)$$

Institute for Microelectronics, TU Wien, Gusshausstrasse 27-29, 1040 Wien, Austria. E-mail: mauro.ballicchia@tuwien.ac.at

The dependence of the position and momentum variables **r** and **p** is inherited from the spatial dependence of **E**(**r**) and **B**(**r**), while **p** enters *via* the Fourier transform. Moreover, in contrast to the electrostatic counterpart, which has been analyzed and applied for more than three decades to a plethora of quantum transport processes,[22,23] there is limited experience with the properties of the gauge-invariant equation. It is thus desirable to gain first-hand experience by reducing the complexity of the equation. A first step in this direction is based on the fact that for stationary EM conditions and a homogeneous **B**, the I^{F}-term can be neglected. Also, H^{F} introduces the magnetic Lorentz force, while D^{F} can be expressed *via* V_{w} for a stationary **E**.[20] As a homogeneous magnetic field can be associated with the zeroth-order term in the Taylor expansion of **B**(**r**), as a next step, it is reasonable to take into account the next (linear) term in the expansion. Therefore, in what follows, we focus on the effects introduced by a magnetic field with spatial linearity. Therefore, we consider the following physical settings: the dimensionality of the problem is reduced to a two-dimensional electron evolution in the **r** = (x, y)-plane. The inhomogeneous magnetic field is normal to the plane in the z-direction: **B** = (0, 0, $B(y)$). In this way, the Lorentz magnetic force is in the plane. The y-coordinate is chosen along the linearity of **B**, so that $B(y) = B_0 + B_1 y$. The electric field **E**(**r**) has a general spatial dependence. Being stationary, the electric field allows the reintroduction of the Wigner potential $V_{\mathrm{w}}(\mathbf{p}, \mathbf{r})$, a quantity which has been physically well analyzed over the last decades. In section 2, we formulate the corresponding magnetic field aware evolution equation for the Wigner function. An analysis of the operators, which compose the equation, is presented.

In section 3, certain physical effects incorporated into the solution are identified in the case of weak non-linearity. Interesting spatial correlations between the electric and magnetic fields are observed, which affect the process of magnetotunneling.[24,25] They are observed in both density and negativity distributions obtained from the Wigner solution, suggesting the existence of both local and non-local interplays of these fields and indicating effects, which can be used for controlling electron evolution. In particular, different settings of the non-linear magnetic field can be used to guide electron trajectories to a desired region of space. Furthermore, it is shown that certain evolution patterns such as snake trajectories and edge states,[2,26,27] which are expected from classical considerations, are maintained by quantum evolution. They can be used to guide and manipulate an electron state by restraining it in a desired region, splitting the density distribution, or affecting its spreading.

2. Wigner equation for linear magnetic fields

The equation has been initially formulated for the case of both linear electric and magnetic fields (see eqn (25) in ref. 21). A linear electric field can be accounted for either by an accelerating (Newtonian) force or, equivalently, by the corresponding Wigner potential term. This duality has been used to verify certain quantum particle concepts used in the electrostatic Wigner theory.[28] For an electric field with a general spatial shape, it is straightforward to reintroduce the Wigner potential in the evolution equation (using eqn (44) and (45) from ref. 20):

$$\left(\frac{\partial}{\partial t}+\frac{\mathbf{p}}{m}\cdot\frac{\partial}{\partial \mathbf{r}}+\mathbf{F}(B(y))\cdot\frac{\partial}{\partial \mathbf{p}}\right)f_{\mathrm{w}}(\mathbf{p},\mathbf{r}) = \int \mathrm{d}\mathbf{p}' V_{\mathrm{w}}(\mathbf{p}-\mathbf{p}',\mathbf{r}) f_{\mathrm{w}}(\mathbf{p}',\mathbf{r}) + \frac{B_1\hbar^2}{m}\frac{e}{12}\left(\frac{\partial^2}{\partial p_y{}^2}\frac{\partial}{\partial x}-\frac{\partial}{\partial p_x}\frac{\partial}{\partial p_y}\frac{\partial}{\partial y}\right)f_{\mathrm{w}}(\mathbf{p},\mathbf{r}) \quad (1)$$

The left-hand side contains the Liouville operator (Lo($B(y)$)), where **F** is the magnetic Lorentz force $\mathbf{F}(B(y)) = \frac{e}{m}\mathbf{p}\times\mathbf{B}(\mathbf{r}) = \frac{e}{m}(p_y B(y), -p_x B(y), 0)$.† On the right-hand side is the Wigner potential term, followed by a term, which involves higher-order mixed derivatives. Without EM fields, the equation reduces to Lo(0) = 0, which resembles the force-less Vlasov equation. The equation involves Newtonian trajectories; however, the quantum character of the evolution depends on the initial condition:[29] the latter can contain, *e.g.*, negative values in contrast to the classical distribution function. An electric field is accounted for by the Wigner potential term $\mathcal{V}_{\mathrm{w}}$, so that the equation takes the well-known form $\mathrm{Lo}(0) = \mathcal{V}_{\mathrm{w}}$. Lo(0) is associated with force-less Newtonian trajectories; however, this does not challenge the quantum character of the theory: Lo(0) together with $\mathcal{V}_{\mathrm{w}}$ gives rise to interference, non-locality, tunneling, negativity, and oscillatory behavior of f_{w}. The evolution is fully coherent as the theory is fully equivalent to wave mechanics.[29,30] Next, if $B_0 \neq 0$, (1) becomes the homogeneous magnetic field equation discussed in ref. 20 (eqn (49)). The Liouville operator in eqn (1) involves Newtonian trajectories driven by the inhomogeneous magnetic field $B(y) = B_0 + B_1 y$, which affects the interplay with $\mathcal{V}_{\mathrm{w}}$. The last operator with the higher-order derivatives is proportional to B_1. This fact provides the opportunity to discriminate the two operators by considering a small B_1. For large y, the magnitude of the linear component $B_1 y$ can become larger than B_0 so that if both have opposite signs, the sign of the magnetic field $B(y)$ is changed. Furthermore, an analysis of physically relevant settings shows that the higher-order derivative operator can be a few orders of magnitude smaller than the Wigner potential. The latter is characterized by the quantity $\gamma \simeq 10^{14\text{–}15}$ s^{-1},[6] characterizing the electric conditions in nanostructures. This is a quantity equivalent to the total out-scattering rate in Boltzmann transport models, which, for instance, for phonons is $10^{12\text{–}13}$ s^{-1}. These considerations suggest that the interplay of Lo($B(y)$) and V_{w} can give rise to important physical effects which dominate the transport for small B_1 values. Accordingly, we neglect the last row in (1) and consider the equation $\mathrm{Lo}(B(y)) = \mathcal{V}_{\mathrm{w}}$. It resembles the standard Wigner equation, which

† In the Lorentz force, in eqn (1), and in the following, **p** refers to the kinetic momentum instead of the canonical momentum.

is associated with a signed-particle model[6].‡ The signed-particle model represents an electron state by an ensemble of numerical particles. The particles have special features that carry the quantum information; however, they evolve in the phase space over Newtonian trajectories dictated by Lo. Thus the left-hand side of (1) determines the trajectories of the particles in the evolving ensemble so that the effects of the classical Lorentz force (due to the linear magnetic field) are incorporated also in the quantum evolution. This is demonstrated by the existence of snake and edge modes in the quantum evolution considered in the next section: there, we consider the essential cases of magnetotunneling and ways to manipulate the state evolution by choosing different settings for B_0 and B_1. Finally, it is important to highlight that such a level of physical insight is a unique feature of the Wigner formalism.

3 Magnetic field effects in the quantum evolution

Simulations were performed with the open source stochastic code ViennaWD[32,33] based on the signed particles. In general, a magnetic field is able to control the trajectory of a classical charged particle. However, the quantum case has a wave-like nature which needs to be incorporated. This is possible by using a signed-particle model which is a numerical model to describe the evolution of a quantum electron state and, moreover, the magnetic field effect in this evolution. In the following sub-sections, we show and study the effect of applying a non-uniform linear magnetic field to a selection of specific quantum electron state evolution scenarios and we highlight the use of magnetic fields for controlling the electron state. Where possible, we compare to classical transport results, as the Wigner signed-particle model we employ provides a seamless transition to the classical transport picture. A coherent evolution (ballistic transport) is considered to outline the analyzed effects.

In Section 3.1, we analyze a magnetotunneling structure where the electron state interacts with an "electric" potential barrier and an external magnetic field orthogonal to the trajectory. In Section 3.2, we analyze the evolution of a quantum electron state in an electronic waveguide with two opposite external magnetic field configurations, resulting in a so-called snake trajectory and the formation of an edge state, respectively.

3.1 Magnetotunneling

Magnetotunneling refers to the effects of a magnetic field on tunneling processes of an electron state through a single-barrier potential. It has been analyzed in the framework of the Wigner formalism in ref. 34, showing how a coherence pattern remains after a barrier, revealing a sort of the "two-peak" waveform. In other work, magnetotunneling has been investigated in ref. 20 with a comparison between the classical and quantum behaviours in the presence of a uniform magnetic field $B(y) = B_0$. The "classical" behaviour corresponds to treating the potential barrier as a classical electric force. In this case, the particle, having a kinetic energy less than the barrier, is completely reflected. In the quantum case, it was demonstrated that there is tunneling, as was expected, *e.g.*, from ref. 34, but in addition it was shown that the process of transmission (including the interference effects) is clearly affected by the magnetic field. In the following, we are going to deepen this analysis, in particular, studying the case where a non-uniform magnetic field is included in the Liouville operator, *i.e.*, where Lo($B(y)$) includes a non-uniform magnetic field $B(y) = B_0 + B_1 y$, and the barrier is quantum mechanically represented by the Wigner potential $\mathcal{V}_w$.

3.1.1 Simulation setup. The simulation domain is $(x, y) = (40\text{ nm}, 60\text{ nm})$, as shown in Fig. 1–4. A 0.3 eV potential barrier is placed at $y = 30$ nm. The barrier thickness is 1 nm and is physically modeled by the Wigner potential V_w in all shown experiments. The initial condition corresponds to a minimum uncertainty Wigner state $\sigma_x = \sigma_y = 3$ nm, which is periodically injected into the simulation domain from the bottom and evolves towards the barrier with a kinetic energy of 0.1 eV. The initial mean velocity is 0 in the x-direction, so almost all the energy at $t = 0$ fs is directed towards the potential barrier. We consider four cases of $(B_0 B_1)$:

Case 1 is $(B_0 B_1) = (0, 0)$ and represents a reference case for the entire experiment since it allows to analyse quantum tunneling through the barrier without the influence of an external magnetic field.

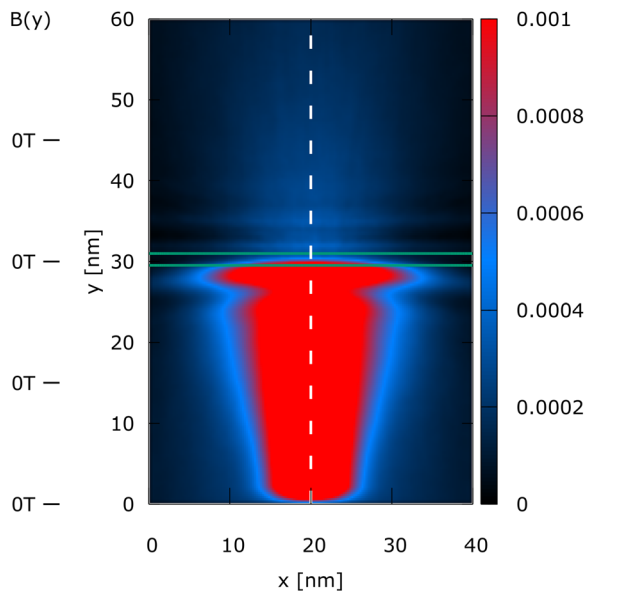

Fig. 1 Case 1: the steady-state electron density, $n(x, y)$, of a Wigner state (electron) injected at the bottom, evolving towards the $+y$-direction. No magnetic field is applied (see $B(y)$ indicators on the left). The dashed line indicates the mean path of the state's evolution. The green lines indicate a 1 nm thick barrier of 0.3 eV. The density shows a fine oscillatory structure above the barrier.

‡The inclusion of the higher-order derivative terms demands an advanced quantum particle model, which is currently in development.[31]

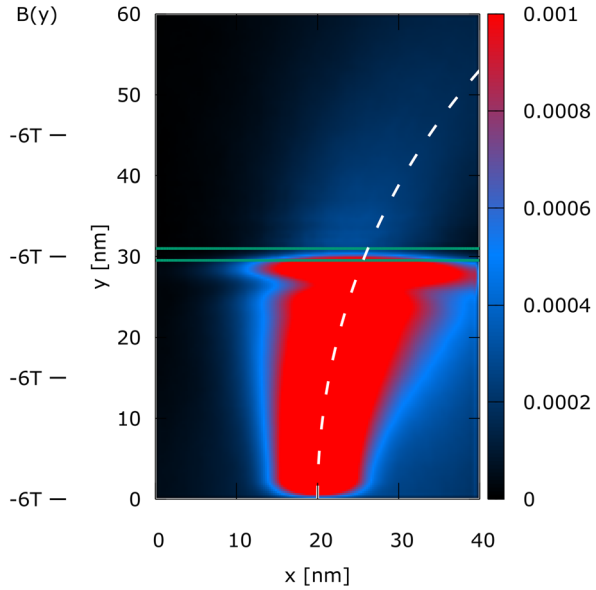

Fig. 2 Case 2: the steady-state electron density, $n(x, y)$, of a Wigner state (electron) injected at the bottom under a constant magnetic field (see $B(y)$ indicators on the left), which bends the density and thus the mean path, indicated by the dashed line. The oscillatory structure above the barrier is strongly reduced by the magnetic field.

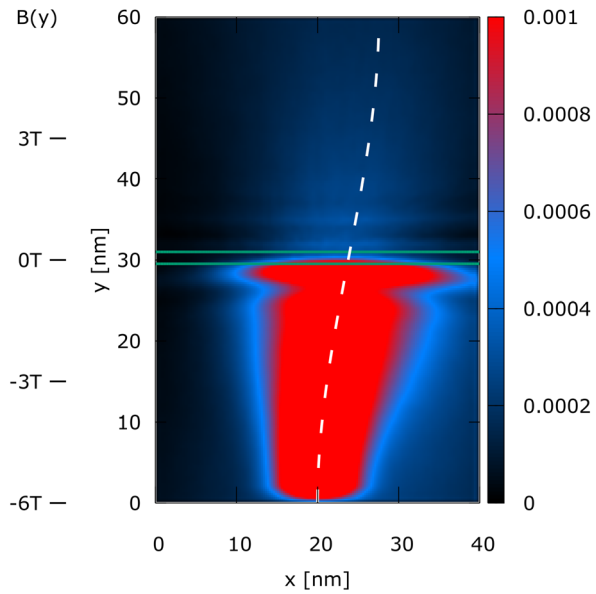

Fig. 3 Case 3: the steady-state electron density, $n(x, y)$, of a Wigner state (electron) injected at the bottom under a linear magnetic that goes from −6 T to 6 T (see $B(y)$ indicators on the left) and thus the magnetic field becomes zero at the barrier and switches the sign, giving rise to a snake type of evolution. The density in the upper half of the domain shows again a fine oscillatory structure.

Case 2 is $(B_0B_1) = (-6\ \mathrm{T}, 0)$ and represents the effect of a uniform magnetic field directed orthogonal to the simulation domain.

Case 3 is $(B_0B_1) = (-6\ \mathrm{T}, 0.2\ \mathrm{T\ nm^{-1}})$. The magnetic field changes its sign around the barrier; the magnetic field is thus zero at the barrier.

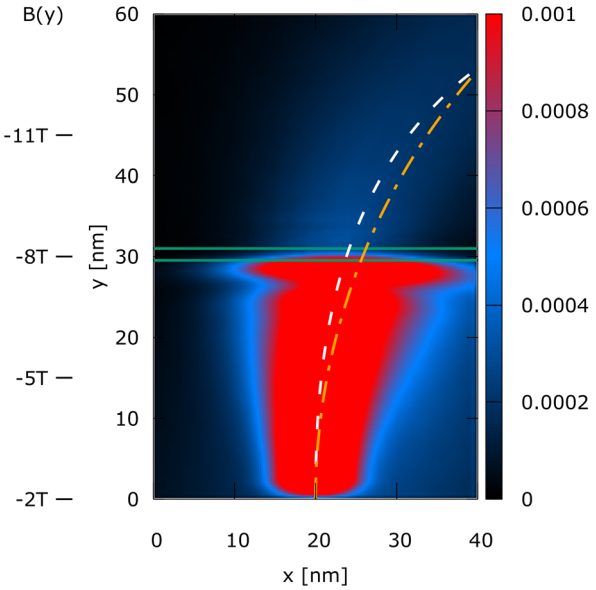

Fig. 4 Case 4: the steady-state electron density, $n(x, y)$, of a Wigner state (electron) injected at the bottom. The magnetic field is gradually increased towards the $+y$-direction and is particularly large at and above the barrier (see $B(y)$ indicators on the left). The magnetic field suppresses the oscillations of the density, similar to case 2. The mean path (white dashed line) is compared to the mean path of case 2 (orange dot-dashed line): Although they differ, they both guide the state to the same final position.

Case 4 is $(B_0B_1) = (-2\ \mathrm{T}, -0.2\ \mathrm{T\ nm^{-1}})$. The linear component B_1y increases the effect of the magnetic field **B** along y, so that the magnitude of the magnetic field is non-zero in the region of the barrier.

3.1.2 Density and negativity analysis. Fig. 1–4 show the electron density for all the four cases. The steady-state electron density, $n(x, y)$, is obtained by the integration over p of the steady-state Wigner function $f_w(\mathbf{x}, \mathbf{p})$. In accordance with the Ehrenfest theorem, in all the four cases, the mean densities follow the classical paths that are indicated by the dotted lines.

In Fig. 1, which is related to $B(y) = 0$, the classical path is the central line $x = 20$ nm, since no magnetic field bends the trajectory. The density perfectly reflects the symmetry with respect to the central dashed line and shows a fine oscillatory structure above the barrier after the tunneling. The latter is almost completely destroyed by the constant magnetic field, as shown in Fig. 2. Therefore, the magnetic field bends the path, guiding the electrons towards a specific position, where considering possible applications, an additional channel could be envisioned, outlining a possible use-case for single-electron control.

In case 3, the magnetic field changes its sign around the barrier, giving rise to a snake type of evolution,[1] as shown in Fig. 3. Besides, the fine structure of the density above $y = 30$ nm is recovered, similar to the case shown in Fig. 1. Observing that the magnetic field is zero at the barrier as in Fig. 1, we associate this effect with the existence of a local

interplay with the EM fields. Indeed, in Fig. 4, when $B(y)$ around the barrier is particularly large (similar to case 2), the oscillations are again suppressed.

In case 4, the electron density, shown in Fig. 4, is very similar to the electron density of case 2, since the magnetic field is negative in the entire simulation domain, but gradually increases towards the $+y$-direction starting from -2 T until -15 T. The mean path (white dashed line) is compared to the mean path of case 2 (orange dot-dashed line): although they differ, they both guide the state to the same final position. An important observation is that the magnetic field is particularly large at and above the barrier in this case, and indeed it suppresses the oscillations of the density, similar to case 2 (Fig. 2).

Since the linear change of the magnetic field is along the y axis and no significant asymmetries with respect to the classical trajectory are observed along the x axis, to better analyze the four cases, the steady-state electron density $n(x, y)$ has been integrated over x, obtaining the density along y, *i.e.*, $n(y)$. One of the advantages of the Wigner formalism and, in particular, of the signed-particle model is to have access to the Wigner function and its negativity obtained by $\mathrm{Neg_w}(\mathbf{r}, \mathbf{p}) = f_w\theta(-f_w)$, where θ is the Heaviside function. The Wigner function negativity indicates the quantum behavior of a state.[35] We thus also investigated the negativity along y, $\mathrm{Neg_w}(y)$, integrating over the momentum $\mathbf{p}$ and over x.

From the comparison of $n(y)$ shown in Fig. 5, it is possible to notice that the oscillatory behaviour in case 1 is smaller than in case 2 before the barrier. It is almost completely destroyed by the magnetic field after the barrier in case 2; only a small variation related to the first two peaks is slightly visible, while in case 1 it is well visible. A further confirmation of the action of the magnetic field on the oscillatory behaviour is given by the fact that case 3, where the magnetic field is almost zero around the potential barrier, behaves similar to case 1, while in case 4, where the magnetic field is even stronger than -6 T, the behaviour is very similar to case 2. This observation strongly suggests the existence of a local effect of the magnetic field on the process of tunneling.

The negativity, as shown in Fig. 6, demonstrates an oscillatory behaviour around the barrier, which is a manifestation of quantum effects. The appearance of negative values after the injection of the entirely positive initial state below the barrier ($y < 25$ nm) demonstrates the non-local action of the barrier already without a magnetic field. The oscillations of the negativity are well visible after the barrier for cases 1 and 3, while they are drastically reduced for cases 2 and 4: only the first two peaks are slightly visible as a change of the slope (gradient). In any case, the negativity shows this behaviour more evidently than the density. This observation provides a confirmation that the magnetic field tends to destroy the oscillatory behaviour of tunneled electrons and also confirms the results presented in ref. 34. It is also possible to observe that the negativity increases with the magnitude of the magnetic field already far before the barrier, which can be seen in all the cases where a magnetic field is different from zero, *i.e.*, cases

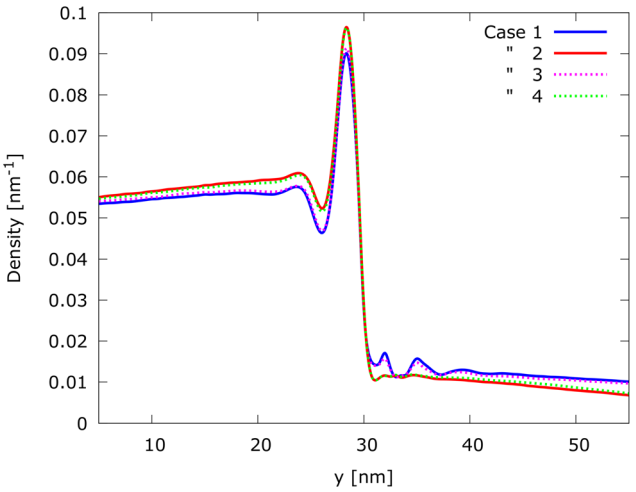

Fig. 5 Density distribution along the y-direction $n(y)$: cases 1 & 3 and 2 & 4 clearly group together, suggesting that the oscillations are suppressed in the presence of a magnetic field in the region of the barrier, further indicating that the EM fields interact locally.

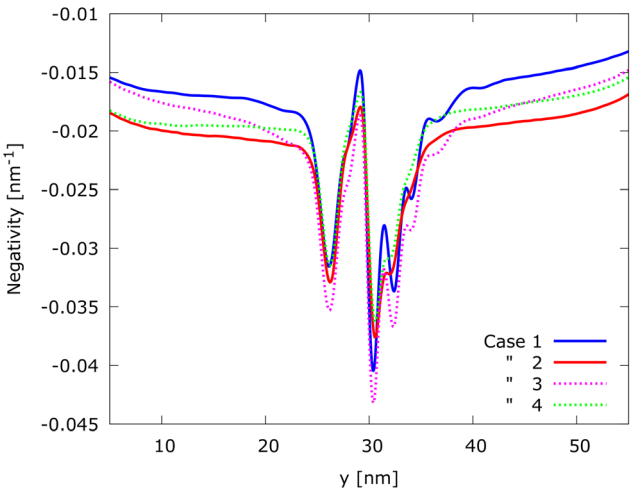

Fig. 6 Negativity along the y-direction $\mathrm{Neg_w}(y)$. Negative values after the injection ($y < 25$ nm) demonstrate the non-local action of the barrier already without a magnetic field. The negativity increases with the increase of $B(y)$ in this region, which suggests again a non-local interplay of the EM field. Oscillatory behavior is slightly visible for the first two peaks in the presence of a strong magnetic field: cases 2 and 4.

2, 3, and 4. This suggests another non-local effect of the interplay of the EM fields.

3.2 Snake trajectory and edge state

In this section, we are going to explore the ability of a non-uniform magnetic field to control the evolution of an electron state not only in terms of trajectory and interference patterns, as in the magnetotunneling application, but also in terms of shape and dispersion of the wave packet. In particular, we are identifying two opposite configurations of the linear magnetic field where the first contributes to maintain the localization of

the wavepacket, as it happens in the case of a snake trajectory, and the second to de-localize, which gives rise to the creation of an edge state.

3.2.1 Simulation setup. In the two following experiments, we consider a portion of an electronic waveguide in the plane x–y with a magnetic field, $\mathbf{B}(\mathbf{r})$, that is orthogonal to the plane x–y and presents a linear dependence in the x-direction, which is orthogonal to the electron evolution (electron state evolves along y). The waveguide width is 600 nm along the x-direction. The magnetic field is defined by $\mathbf{B}(\mathbf{r}) = (0, 0, B(x))$ with $B(x) = B_0 + B_1 x$. Eqn (1), which describes the electron state evolution, keeps the same form except that y and x are exchanged. The waveguide length for the snake trajectory and edge state experiment is 2500 nm and 3000 nm, respectively. We evolved a minimum uncertainty Wigner state with $\sigma_x = \sigma_y = 36$ nm, $m_{\text{eff}} = 0.19m_e$ and an initial energy of 0.045 eV along y. The electron state is placed at $y_0 = 300$ nm and we used a Gaussian state that is fully included in the simulation domain at $t = 0$.

3.3 Snake trajectory

In the snake trajectory experiment, the value of the magnetic field is defined by $B_0 = -1$ T and $B_1 = 0.0033$ T nm^{-1}. This means that the magnetic field starts at -1 T at $x = 0$ nm and increases to 1 T at $x = 600$ nm and is constant along the y-direction, as shown in the right part of Fig. 7. The initial position of the Wigner state is $(x_0, y_0) = (370$ nm, 300 nm) and is placed 70 nm to the right of the waveguide center which is at $x = 300$ nm, where $B = 0$ T, see Fig. 7.

The left part of Fig. 7 shows the evolution of the electron state along the waveguide. Fig. 7 shows the density of the quantum states in specific time instants $t = 0$ ps, 1.6 ps, 3.2 ps, 5.0 ps, and 6.4 ps. The dashed white line represents the trajectory of a classical "point-like" particle that evolves along the wire starting from the middle of the quantum state with the same mean velocity. Furthermore, the chosen magnetic field affects the shape of the electron state, as shown by the distribution of the electron density. At $t = 0$, the state is perfectly circular. During the evolution, the width of the wavepacket is affected by the magnetic field. In particular, along the x-direction the "width" of the wavepacket tends to decrease, approaching the center ($t = 1.6$ ps), followed by an increase again as it oscillates to the other side ($t = 3.2$ ps). This is due to the non-uniform magnetic field along x that tends to concentrate the density along the $B(x) = 0$ line. Fig. 8 shows the evolution of variances Δx and Δy of the spread of the packet in the x and y directions, as compared to the variance of a freely evolving wavepacket. Particularly interesting is the behavior of Δx, which is kept bounded around the initial value by the magnetic field. The different behaviour of Δx and Δy is due to the different behaviour of the Lorentz force that causes the wavepacket to oscillate along x and to move forward along y.

3.4. Edge state

In the edge state experiment, the magnetic force is opposite to the one used in Section 3.3, as can be seen from the right part of Fig. 9. Thus $B_0 = 1$ T and $B_1 = -0.0033$ T nm^{-1}, so the magnetic field ranges from 1 T to -1 T along x and is constant along the y-direction. The initial position of the Wigner state ($t = 0$ ps) is perfectly centered, *i.e.*, $(x_0, y_0) = (300$ nm, 300 nm), where $B = 0$ T, as can be seen in the left part of Fig. 9. In the classical case, a particle evolving in the center and along the line $x = 300$ nm (where the magnetic force is zero) will not be affected by the action of the magnetic field. In the quantum case, the electron state density is distributed in space, according to Heisenberg's uncertainty principle, and represented by an ensemble of numerical particles, so that the evolution is

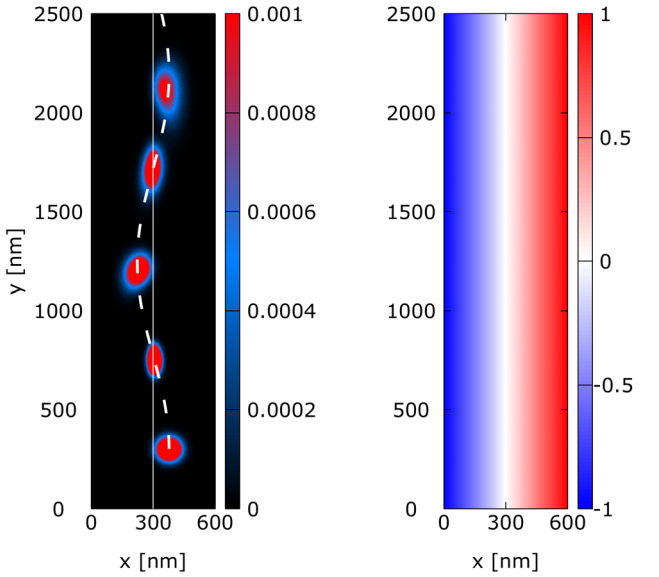

Fig. 7 Snake trajectory: evolution of a minimum uncertainty Wigner state along a waveguide under an orthogonal, non-uniform linear magnetic field $B(x) = B_0 + B_1 x$ with $(B_0 B_1) = (-1$ T, 0.0033 T nm$^{-1})$. The right part shows the magnetic field $B(x)$ in tesla (T). The left part shows the electron density at $t = 0$, 1.6 ps, 3.2 ps, 5 ps, and 6.4 ps. The electron state follows a snake trajectory indicated by the white dashed line.

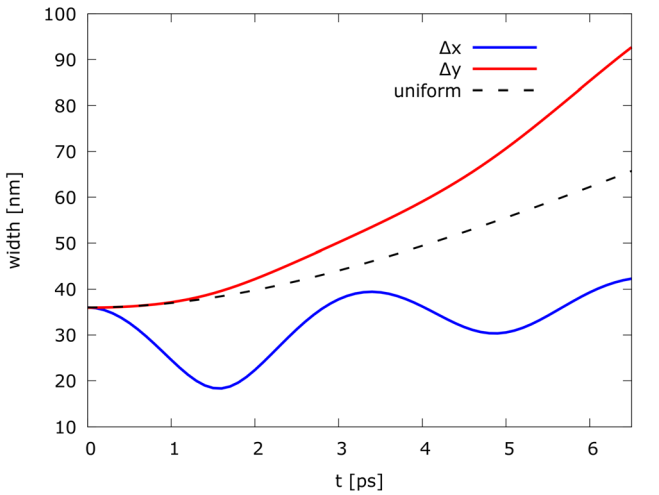

Fig. 8 Evolution of variances Δx and Δy of the spread of the Gaussian wavepacket in the x and y directions, as compared to the variance of a freely evolving (uniform motion) wavepacket indicated by the dashed line.

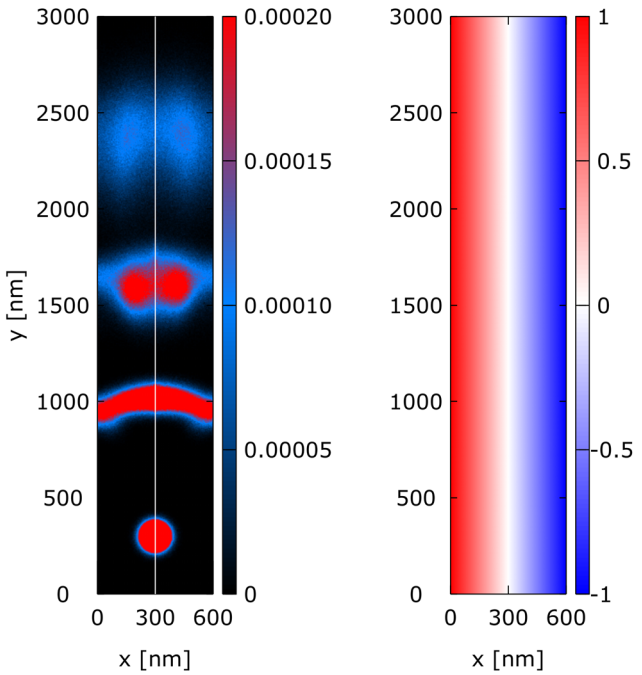

Fig. 9 Edge state: evolution of a minimum uncertainty Wigner package along a waveguide under an orthogonal non-uniform linear magnetic field $B(x) = B_0 + B_1x$ with $(B_0B_1) = (1\ \mathrm{T}, -0.0033\ \mathrm{T\ nm^{-1}})$. The right part shows the magnetic field $B(x)$ in tesla (T). The left part shows the electron density at t = 0, 2.5 ps, 5 ps, and 8 ps. At the end, the wavepacket becomes a split edge state.

always affected by the action of the magnetic field. It is thus clear that in the quantum case, the signed-particle model is useful as it allows to describe and heuristically understand the electron evolution. Parts of the electron density on the left of the central line are pushed towards the left border of the waveguide, while other parts on the right are pushed towards the right border. The boundary conditions reflect the parts of the split state back towards the center. An analysis of the left part of Fig. 9 shows the density of the quantum states at specific times t = 0 ps, 2.5 ps, 5.0 ps, and 8.0 ps. As we can see at t = 2.5 ps, the electron density width increases along the x-direction during the evolution. This dispersion is driven by the Lorenz force and provides a curvilinear shape along x to the wavepacket, similar to an "arc". When the electron state interacts with the lateral borders of the waveguide, it is reflected towards the center, this can be seen by the fact that the bending of the curvilinear shape disappears near the borders. At t = 5.0 ps, the electron state is completely reflected and the density takes an almost "bimodal distribution" form along x. It is almost separated in two parts, one on the left and one on the right of the line x = 300 nm, where the magnetic field is zero. Only a small portion of the density is still in the center of the waveguide. The electron density at t = 8.0 ps keeps the bimodal distribution which is more defined and evolves along the waveguide as two parallel parts of an edge state that travel in the same direction, due to the opposite sign of the magnetic field. This behaviour is further confirmed by the dispersion of the two parts along the direction of motion that is clearly visible comparing to the density at t = 5.0 ps with the density at t = 8.0 ps. This configuration of the magnetic field splits the state and pushes its parts towards the boundaries which reflect them back. This mechanism of electron splitting can be an attractive option for research in electron quantum optics, where "beam splitter" concepts are a vital building block.

4 Summary

Non-uniform magnetic fields offer unique capabilities to control single electron states. Here, we investigated a generalization of eqn (25) proposed in ref. 21 for non-linear electric fields. The obtained equation involves the conventional Wigner potential, the magnetic Lorentz force that also includes linear magnetic fields, and higher-order terms that depend on the linear coefficient of **B**. The higher-order terms can be neglected for small magnitudes which allows us to perform numerical calculations in terms of the well-developed signed-particle model. Experiments on magnetotunneling and, in particular, the capability of linear, non-uniform magnetic fields to control an electron state trajectory are shown. Moreover, the possibility of changing the value of the magnetic field allows us to specifically influence an interference pattern or an oscillatory behaviour. We also show the capability of linear, non-uniform magnetic fields to control the spatial dispersion of an electron state or to split the electron state. It should be stressed that both cases of evolution have a classical analog of evolving initial Gaussian distributions of an ensemble of non-interacting electrons. Indeed, for the considered physical setup, classical and quantum evolution rules are the same. However, in the former, the initial condition can only be non-negative, while in the latter, negative values are also possible, characterising the Wigner quasi-distribution function.

Conflicts of interest

There are no conflicts to declare.

Acknowledgements

This research was funded in whole or in part by the Austrian Science Fund (FWF) [10.55776/P33609, 10.55776/P37080]. For open access purposes, the author has applied a CC BY public copyright license to any author accepted manuscript version arising from this submission. The computational results have been achieved using the Vienna Scientific Cluster (VSC).

References

1 P. Hoodbhoy, *J. Phys.: Condens. Matter*, 2018, **30**, 185303.
2 P. Mondal, A. Nogaret and S. Ghosh, *Phys. Rev. B*, 2018, **98**, 125303.

3 X. Zhang and Y. Liu, *Phys. Lett. A*, 2020, **384**, 126613.
4 C. Karmakar, R. Kaneriya, G. Rastogi, R. Upadhyay, P. Kumar and U. Joshi, *Phys. Lett. A*, 2021, **417**, 127693.
5 P. Hoodbhoy, *J. Phys.: Condens. Matter*, 2020, **33**, 065601.
6 M. Nedjalkov, D. Querlioz, P. Dollfus and H. Kosina, in *Wigner Function Approach*, ed. D. Vasileska and S. M. Goodnick, Springer New York, New York, NY, 2011, pp. 289–358.
7 W. V. Houston, *Phys. Rev.*, 1940, **57**, 184–186.
8 B. Novakovic, R. Akis and I. Knezevic, *Phys. Rev. B: Condens. Matter Mater. Phys.*, 2011, **84**, 195419.
9 J. B. Krieger and G. J. Iafrate, *Phys. Rev. B: Condens. Matter Mater. Phys.*, 1986, **33**, 5494–5500.
10 I. B. Levinson, *Sov. Phys. JETP*, 1970, **30**, 362–367.
11 R. Kubo, *J. Phys. Soc. Jpn.*, 1964, **19**, 2127–2139.
12 F. Rossi, in *Bloch Oscillations and Wannier–Stark Localization in Semiconductor Superlattices*, ed. E. Schöll, Springer, Boston, 1998, pp. 283–320.
13 G. J. Iafrate, V. N. Sokolov and J. B. Krieger, *Phys. Rev. B*, 2017, **96**, 144303.
14 T. B. Materdey and C. E. Seyler, *Int. J. Mod. Phys. B*, 2003, **17**, 4555–4592.
15 T. B. Materdey and C. E. Seyler, *Int. J. Mod. Phys. B*, 2003, **17**, 4683–4732.
16 L. Bellentani, P. Bordone, X. Oriols and A. Bertoni, *Phys. Rev. B*, 2019, **99**, 245415.
17 L. Avazpour, M. King, S. Belling and I. Knezevic, International Conference on Numerical Simulation of Optoelectronic Devices (NUSOD), 2022, pp. 111–112.
18 R. Stratonovich, *Dokl. Akad. Nauk SSSR*, 1956, **109**, 72–75.
19 O. T. Serimaa, J. Javanainen and S. Varró, *Phys. Rev. A*, 1986, **33**, 2913–2927.
20 M. Nedjalkov, J. Weinbub, M. Ballicchia, S. Selberherr, I. Dimov and D. K. Ferry, *Phys. Rev. B*, 2019, **99**, 014423.
21 M. Nedjalkov, M. Ballicchia, R. Kosik and J. Weinbub, *Phys. Rev. A*, 2022, **106**, 052213.
22 D. Querlioz and P. Dollfus, *The Wigner Monte Carlo Method for Nanoelectronic Devices*, Wiley, 2013.
23 D. K. Ferry and M. Nedjalkov, *The Wigner Function in Science and Technology*, IOP Publishing, 2018.
24 L. Pratley and U. Zülicke, *Phys. Rev. B: Condens. Matter Mater. Phys.*, 2013, **88**, 245412.
25 N. Prasad, G. W. Burg, K. Watanabe, T. Taniguchi, L. F. Register and E. Tutuc, *Phys. Rev. Lett.*, 2021, **127**, 117701.
26 J. E. Müller, *Phys. Rev. Lett.*, 1992, **68**, 385–388.
27 J. Reijniers and F. M. Peeters, *J. Phys.: Condens. Matter*, 2000, **12**, 9771.
28 M. Nedjalkov, P. Schwaha, S. Selberherr, J. M. Sellier and D. Vasileska, *Appl. Phys. Lett.*, 2013, **102**, 163113.
29 N. C. Dias and J. N. Prata, *Ann. Phys.*, 2004, **313**, 110–146.
30 V. I. Tatarskiĭ, *Soviet Phys. Usp.*, 1983, **26**, 311.
31 C. Etl, M. Ballicchia, M. Nedjalkov and J. Weinbub, *J. Phys. A: Math. Theor.*, 2024, **57**, 115201.
32 P. Ellinghaus, J. Weinbub, M. Nedjalkov, S. Selberherr and I. Dimov, *J. Comput. Electron.*, 2015, **14**, 151–162.
33 ViennaWD, **https://www.iue.tuwien.ac.at/viennawd/**, [accessed: 12/04/2024].
34 N. C. Kluksdahl, A. M. Kriman and D. K. Ferry, *High Magnetic Fields in Semiconductor Physics II*, Berlin, Heidelberg, 1989, pp. 335–338.
35 M. Ballicchia, D. K. Ferry, M. Nedjalkov and J. Weinbub, *Appl. Sci.*, 2019, **9**, 1344.